Performance evaluation of the integrating system of TS-MSR and SOFC: effect of microchannel technology on the thermo-chemo-mechanical behavior of TS-MSR

LI Zheng [1], YANG Guogang [1*], ZHANG Guoling [1], LIAO Jiadong [1], JIANG Ziheng [1], WANG Hao [1]

1 Marine Engineering College, Dalian Maritime University, Dalian 116026, China.

*Corresponding author: E-mail: yanggg@dlmu.edu.cn (G. Yang);

ABSTRACT

In previous work, we proposed an integrated system of solid oxide fuel cells (SOFCs) and thermally self-sustained methane steam reformer (TS-MSR) and conducted the corresponding thermo-electro-chemo-mechanical behavior evaluation of SOFCs considering pre-reformer designs. While this work aims to conduct the thermo-chemo-mechanical behavior evaluation of TS-MSR when micro-channel technology is employed. The results indicate the application of microchannel technology facilitates the mass transfer within the TS-MSR and the resulting lower temperature improves the thermal strain stress behavior. This study can provide a reference for the design and thermomechanical evaluation of the integrated system before commercialization.

Keywords: SOFC, TS-MSR, hydrogen, microchannel technology, thermo-chemo-mechanical behavior

NONMENCLATURE

Abbreviations	
TS-MSR	Thermally self-sustained methane steam reformer
SOFC	Solid oxide fuel cell

1. INTRODUCTION

Increasing evidence has identified the irreversible damage to the planet caused by the global warming [1] and a growing number of countries have announced pledge to reach carbon neutral in the coming decades. Consequently, fuel cells enjoy a revival in recent years where solid oxide fuel cell (SOFC) is highly expected due to its fuel flexibility and easier deployment (backed with existing natural gas pipeline network) to hedge the high cost of producing, storing and transporting pure hydrogen.

However, feeding methane directly into SOFCs typically leads to two issues: (1) coke deposition which blocks surface active sites and causes a serious performance degradation [2]; (2) the formation of a significant temperature gradient at inlet region which enhances thermal stresses and induces possibly micro-cracks on brittle ceramic materials of the fuel cell [3]. Therefore, in previous work [4], we proposed an integrated system of SOFCs and TS-MSR to increase its lifespan and improve its the comprehensive thermal efficiency, wherein the design of TS-MSR becomes essential.

The development of microchannel technology provides an opportunity for the miniaturization and integration of reformers which is of paramount importance for on-board application such as a fuel cell ship. Reduction of characteristic size in diffusion direction could bring a process intensification simultaneously on heat and mass transfer. As such, available [5-8]literatures have suggested lower channel size in diffusion direction by micro manufacturing technology.

However, TS-MSR operates at high temperature and the resulting thermal impact would induce thermal strain stresses. The corresponding thermo-mechanically induced stress would cause the material failure, catalyst layer delamination and exfoliation, eventually lead to the failure of stack operation in practice. This problem becomes more significant when microchannel size was employed. An arbitrary maximum temperature of 1500K [9] or 1400K [10] are usually adopted as the materials stability limit in available literatures. This criterion was given empirically. The corresponding detailed evaluating of thermo-mechanically induced stress behavior was required.

Therefore, a three-dimensional computational fluid dynamics model coupling chemical reaction and thermal strain stress of TS-MSR was developed in this work. The numerical analysis is focused on the thermal characteristic and thermo-mechanically induced stress behavior when micro-channel technology is employed. This study can provide a reference for the design and

thermomechanical evaluation of the integrated system before commercialization.

2. MATHEMATICAL MODELLING DESCRIPTION

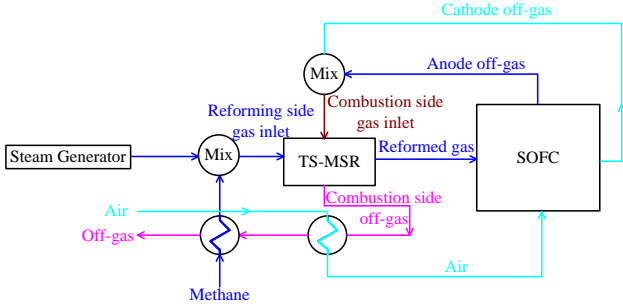### 2.1 System configuration and computational domain description

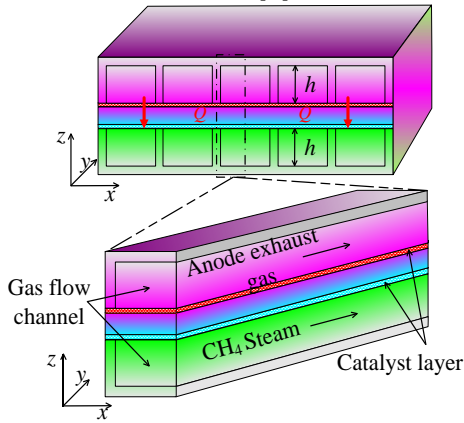Fig.1 (a) Schematic diagram of integrated SOFCs with TS-MSR [4]

Fig.1 (b) Schematic representation of computational domain for the simulation of TS-MSR

As shown in Fig.1(a), to reduce carbon deposition and avoid unnecessary temperature gradients at the entrance of SOFCs, we proposed an integrated system of SOFCs and TS-MSR and conducted the corresponding thermo-electro-chemo-mechanical behavior evaluation of SOFCs considering pre-reformer designs in our previous work [4]. While this work aims to conduct the thermo-chemo-mechanical behavior evaluation of TS-MSR when micro-channel technology is employed and the corresponding schematic diagram is shown in Fig. 1(b). As shown in Fig. 1(b), TS-MSR mainly consists of three parts: the adjacent multichannel, the substrate plate (where catalyst layer was coated) and the interconnecting ribs (to support the channel structure). The reforming channels and catalytic combustion channels were neatly aligned and separated by the substrate plate. In reforming channels, activated by Ni-based catalyst, methane and steam were converted into hydrogen-rich gas during reforming reaction. The required heat consumption of endothermic reforming

reaction was supported by catalytic anode exhaust gas combustion of combustion channels in the presence of Pt-based catalyst. This stackable form was considered as one of the most potential forms due to its convenience in modularization adjusted to hydrogen demand. For a stacked plate reformer, the alternated channels for reforming and combustion allows researchers to impose the symmetry conditions in their investigations. Therefore, as shown in Fig.1 (b), a set of adjacent half channel consisting of a reforming flow channel and a combustion flow channel was employed as the computational domain. The detailed geometry parameter of the computational domain is shown in Table 1.

Table 1 Geometry parameter of the computational domain.

	Reforming duct	Combustion duct
Channel height (mm)	0.25-3	0.25-3
Catalyst layer thickness (mm)	0.02	0.02
Substrate plate thickness (mm)	0.5	0.5
Length(cm)	30	30
Width (mm)	1	1

2.2 Model description

Before conducting the simulation, a few assumptions were made as follows:

(1) The reformer is in a steady operation.

(2) The reactant gas is considered as compressible ideal gas (high temperature and low-pressure conditions).

(3) Flow remains laminar in both half-channels.

(4) Radiative heat transfer is neglected.

(5) Both catalyst coating and solid material are isotropic.

(6) Materials in this model meet the linear elastic theory.

2.2.1 Governing equations

Corresponding to the respective regions, the governing equations are as follows:

For reforming and combustion flow-channels, Navier-Stokes equations based numerical model was adopted:

$$\nabla\left(\rho\vec{u}\right)=0 \tag{1}$$

$$\left(\rho \cdot \nabla \cdot \vec{u}\right) \cdot \vec{u} - \nabla \left\{ -p + \left[\psi + \frac{2\mu}{3}(\nabla) \cdot \vec{u} \right] \right\} = \mathbf{F} \quad (2)$$

$$\rho \cdot c_p \cdot \vec{u} \cdot \nabla T - \nabla \cdot \left(k_{\text{mix}} \nabla T \right) = 0 \quad (3)$$

$$\rho(\vec{u}\nabla) \cdot \omega_i - \nabla \left\{ \rho \omega_i \sum D_{ij} \left[\nabla x_k + \frac{1}{p}\left[(x_k - \omega_k)\nabla p \right] \right] \right\} = \sum r_i M_j \quad (4)$$

For porous catalyst layer, the modified Navier-Stokes equation by Darcy's term and porosity was adopted to describe the momentum conservation. In equation (8), the modified Fick model instead of Dusty Gas model was adopted due to its superior performance under the trade-off between the accuracy and requirement to calculation resource. The heat source and mass sources derived from the chemical reaction (the reaction kinetics could be found in our previous work [11]) was attributed to rightmost terms:

$$\nabla \left(\rho \vec{u} \right) = 0 \quad (5)$$

$$\left(\frac{\mu}{\kappa} + \rho \cdot \nabla \cdot \vec{u} \right) \cdot \vec{u} - \nabla \left\{ -p + \frac{1}{\varepsilon}\left[\psi + \frac{2\mu}{3}(\nabla) \cdot \vec{u} \right] \right\} = \mathbf{F} \quad (6)$$

$$\rho \cdot c_p \cdot \vec{u} \cdot \nabla T - \nabla \cdot \left(k_{\text{eff}} \nabla T \right) = \sum r_i H_i \quad (7)$$

$$\rho(\vec{u}\nabla) \cdot \omega_i - \nabla \left\{ \rho \omega_i \sum D_{\text{eff},ij} \left[\nabla x_k + \frac{1}{p}\left[(x_k - \omega_k)\nabla p \right] \right] \right\} = \sum r_i M_j \quad (8)$$

For solid wall:

$$\nabla \cdot \left(k_{\text{w}} \nabla T \right) = 0 \quad (9)$$

2.2.2 Thermal stress coupling

The thermal expansion caused by uneven temperature distribution would induce the corresponding thermal strain. This thermal strain consequently was calculated as:

$$\varepsilon_{\text{th}} = \alpha \left(T - T_{\text{ref}} \right) \quad (10)$$

where α is the thermal expansion coefficient of the corresponding material, T_{ref} represents the zero thermal stress state and is adopted as the spraying temperature.

The thermal stress (σ) was calculated by the thermal stain and mechanical properties of the materials:

$$\sigma = \varepsilon_{\text{th}} D \quad (11)$$

where D is the elasticity matrix:

$$D = \frac{E}{(1+v)(1-2v)} \begin{bmatrix} 1-v & v & v & 0 & 0 & 0 \\ v & 1-v & v & 0 & 0 & 0 \\ v & v & 1-v & 0 & 0 & 0 \\ 0 & 0 & 0 & \frac{1-2v}{2} & 0 & 0 \\ 0 & 0 & 0 & 0 & \frac{1-2v}{2} & 0 \\ 0 & 0 & 0 & 0 & 0 & \frac{1-2v}{2} \end{bmatrix} \quad (12)$$

where E is the Young's modulus and v is the Poisson ratio of the material.

2.3 Solution method and model validation

The proper boundary conditions were required to solve the numerical model of TS-MSR under working condition. For a concise presentation, the boundary conditions of the simulation were summarized in Table 2. The inlet temperature is assumed as 793 K, the inlet species is 30% pre-reformed natural gas and the operating pressure is atmosphere. In addition, the Fe-Cr-Al alloy was chosen as manufacturing materials. All these parameters and material properties could be found in our previous work [4].

The effect of channel height is the focus when considering the application of micro-channel technology. It was worth mentioning that the gas hourly space velocity should be kept constant when conducted the simulation of different channel heights, which was confirmed by Zafir et. al. [12]. It means keep a constant inlet volume flowrate (92mL/min for reforming reactant and 50mL/min for combustion reactant in present work).

Table 2 The boundary conditions of the simulation model.

Boundary conditions			
Inlet condition	$u_y=u_0$ $u_x=u_z=0$	$T=T_0$	$\omega=\omega_{i,0}$
Outlet condition	$p=p_0$	$\nabla T = 0$	$\nabla \omega = 0$
The upper, lower and lateral wall of solid domain	$u_x=u_y=u_z=0$	$\nabla T = 0$	$\nabla \omega = 0$
The lateral wall of flow-channel	$\nabla u = 0$	$\nabla T = 0$	$\nabla \omega = 0$

This work is an extension of our previous work [4]. A detailed grid-independence verification and model validation have already been conducted and introduced in that work. For a concise presentation, it was only briefly described in this section. As mentioned in that work, this model was solved in COMSOL Multiphysics with a fine mesh (8.58×10^5 cells where a grid independent solution is available). We also compared the numerical results with the experimental data of Shu et. al. [13] in detail and the simulation data of Zafir et. al. [12] for a model validation. All comparisons show a satisfying agreement.

3. RESULTS AND DISSCUSSIONS

3.1 Evaluating of the output performance

The methane conversion rate and hydrogen yield are considered as the key performance indexes for TS-MSR because maintaining low operating temperatures at the expense of low conversion rate is achievable but of no application value. Fig.2 shows the methane conversion rate and hydrogen yield of the reformer under different channel heights. It can be seen the methane conversion inside the reforming duct of the reactor under varied channel heights in present work is higher than 65%. The methane conversion of reforming duct is 66.4% when channel height is 3mm. While the conversion is 83.1% when channel height is 0.5mm. It means methane conversion was increased by 16.7% when channel height is decreased from 3mm to 0.5mm thanks to the shorter diffusion path of reactants from flow channel to reaction region of the catalyst layer. The corresponding hydrogen yield is also increase from 23.6% to 27.7%. When channel height further decreases from 0.5mm to 0.25mm, the methane conversion slightly decreases but still reach 80.1%. This may be caused by its lowest temperature when channel height reaches 0.25mm which would be discussed in the thermal characteristic behavior section.
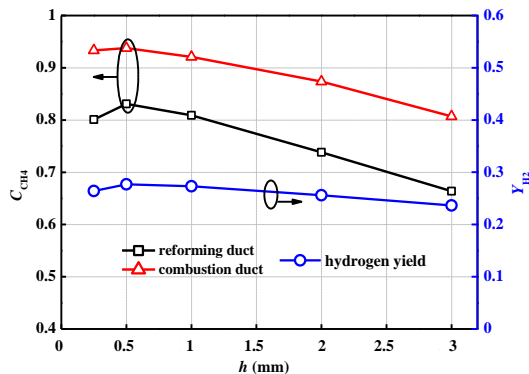

Fig.2 the methane conversion rate and hydrogen yield of the reformer under different channel heights

3.2 Evaluating of heat and mass transfer behavior

As mentioned previously, thermal characteristic is critical for both the performance and operation safety of TS-MSR. Fig.3 shows reforming gas duct temperature contour of TS-MSR under varied channel heights. In order to facilitate comparison, their legends have been standardized. Overall, reformer temperature increases from the inlet to the outlet when channel height is fixed. For varied channel heights, qualitatively, a significant temperature decrease was obtained by decreasing reformer channel height. It can be seen, at the same axial position, temperature remains at the lower value with the reduction of channel height. It implies the lower average temperature and the hotspot can be achieved by

decreasing reformer channel height, which facilitates operation safety of microchannel TS-MSR.
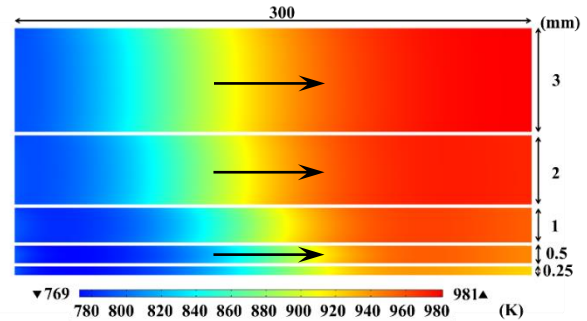

Fig.3 The reformer reforming duct temperature contour under different channel heights

The mass Fourier number was often obtained to evaluate whether the reactant has enough time to diffuse into the catalyst layer before leaving the reformer. It was calculated by the ratio of axial residence time to transverse diffusion time of the fuel. Therefore, taking methane of the reforming duct as an example, its mass Fourier number under different channel heights is plotted in Fig.4. It should be noted that mass Fourier is the ratio of convection space time and diffusion space time. When mass Fourier is greater than 1, i.e., its logarithm is positive, the reactant has enough time to diffuse into the catalyst layer to participate in reaction before leaving the reformer, and vice versa. It can be seen the logarithm of mass Fourier number near the reformer inlet for different channel heights is positive. It indicates the reactant at this position has enough time to diffuse into the catalyst layer before leaving the reformer. However, mass Fourier number becomes negative when x/L exceeds 0.2 for reformer with channel height of 3mm. It implies some of the reactants flows out of the reformer without diffusion into the catalyst layer. And the higher the channel height, the longer the segments with negative mass Fourier number in the reformer. The mass Fourier number for reformer with channel height of 0.25mm turns from positive to negative when x/L reaches 0.92. It implies most of the reactants within the reformer with channel height of 0.25mm can diffuse into the catalyst layer to participate in the reforming reaction. This indicates decreasing the channel height of the reformer facilitates to the reforming reaction from mass transfer point of view.
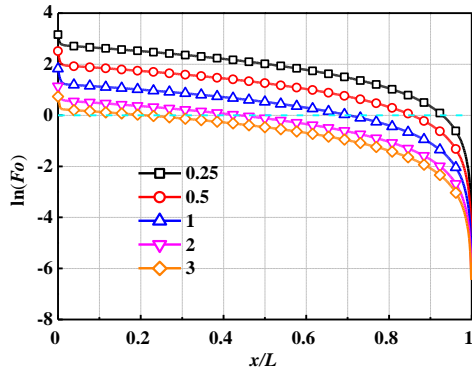
Fig.4 the mass Fourier number distribution of the reforming duct centerline of the reformer under different channel heights

Corresponds to the mass Fourier number under different channel heights, taking methane and hydrogen as examples, Fig.5 shows the species mole fraction contour inside the reforming duct of the reformer. It can be seen in Fig.5(a), the mole fraction of methane inside the reforming duct is not uniform due to the consumption caused by the reforming reaction. Its maximum value at radial direction appears in the lower half of the reforming duct away from the catalyst layer, rather than the centerline of the duct. Its minimum value appears at the interface with the catalyst layer where methane was consumed by reforming reaction. This is because molecule diffusion inside the reforming channel is weaker than the convection. What's more, the lower the channel height, the lower the mole fraction of methane at the same position. Different from methane, as a product, the mole fraction distribution of hydrogen was inverted. The minimum mole fraction of hydrogen, as shown in Fig.5(b), appears in the lower half of the reforming duct. While its maximum value appears at the interface with catalyst layer where hydrogen was produced by reforming reaction. The lower the channel height, the higher the hydrogen mole fraction at the same position. It should be noted the mole flow rate was kept consistent for different channel heights. It implies the consumption rate of methane was increased by the decrease of channel height. In other words, the methane reforming reaction was enhanced by the decrease of channel height.
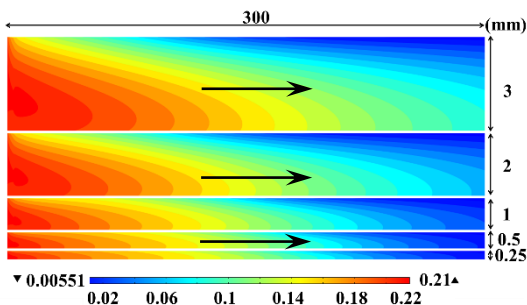

(a) the mole fraction contour of methane
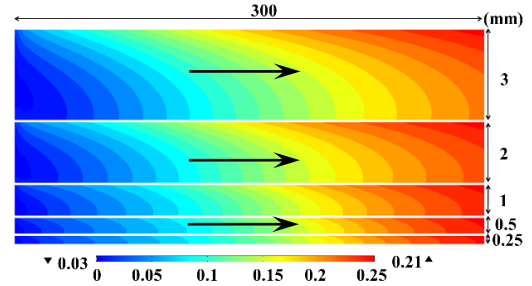
(b) the mole fraction contour of hydrogen

Fig.5 the mole fraction contour inside the reforming duct of the reformer under different channel heights

3.3 Evaluating of thermo-mechanically induced stress behavior

As mentioned before, the thermal expansion attributed to uneven temperature distribution, different thermal expansion coefficients of manufacturing materials and the assembly constraint would induce thermal strain stress and may eventually break down the reformer. Therefore, Fig.6 shows the thermal strain and the corresponding thermal stress of the reformer under varied channel heights.

As can be seen in Fig.6(a), reformer thermal strain contour is similar as its corresponding temperature contour. The thermal strain is usually higher where the temperature is high. Corresponds to the temperature distribution, the thermal strain increases from reformer inlet to its outlet when reformer channel height is fixed. And it is noteworthy that high thermal strain appears in reformer catalyst layer, the vulnerable region, of outlet section. The maximum thermal strain is 0.00887 when channel height is 3mm. This may result in the delamination and exfoliation of catalyst layer, which could in turn cause further thermal runaway and greater strain.

Similar to the effect of channel height on temperature, the maximum thermal strain decreases with the decrease of reformer channel height. The maximum thermal strain is 0.00826, 0.00757 and 0.00695 when channel height is 2mm, 1mm and 0.5mm, respectively. The maximum thermal strain obtained a minimum of 0.00611 when channel height is 0.25mm. It means the thermal strain behavior was improved by decreasing the channel height. The corresponding explanation could also be derived from its temperature distribution. The decrease of channel height obtained a heat and mass transfer intensification and the resulting lower temperature improves the thermal strain behavior. Therefore, from a strain point of view, the reformer temperature should be reasonably controlled, especially to avoid extreme temperatures.

The corresponding thermal stress contours of TS-MSR under different channel heights were shown in Fig. 6(b). Von Mises stress was adopted to evaluate the thermal strain stress behavior of the reformer because it integrates the first, second and third principal stresses to express the critical value of the distortion component of the deformation energy and find the most vulnerable locations of the equipment. Corresponds to the distribution of thermal strain, reformer outlet region appears higher Von Mises stress value when channel height was fixed. It could be inferred reformer outlet region was is more prone to fracture in comparison with the inlet one.

The maximum Von Mises stress appears at the interconnect rib corner of reformer outlet and reaches 1841MPa when channel height is 3mm. It means that more attention should be paid to the design of interconnect rib corner of reformer outlet. When channel height was lowered to 2mm, the Von Mises stress was reduced with the value of 1595MPa. Moreover, the lower the channel height, the lower the maximum Von Mises stress. The maximum Von Mises stress is 1383 MPa and 1306MPa when channel height is 1mm and 0.5mm respectively. When channel height of 0.25mm was adopted, the maximum Von Mises stress was reduced into 1277MPa. It means the maximum Von Mises stress was reduced by 564MPa when channel height decreases from 3mm to 0.25mm. It could be inferred reducing the channel height facilitates the safe operation of TS-MSR. As a consequence, the lower channel height was recommended from safe operation point of view.
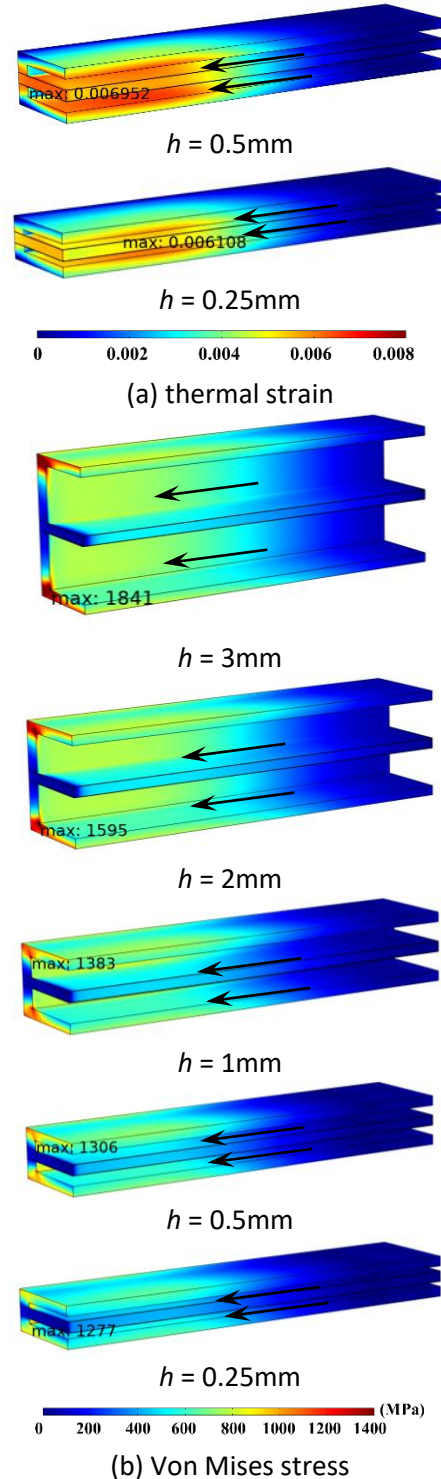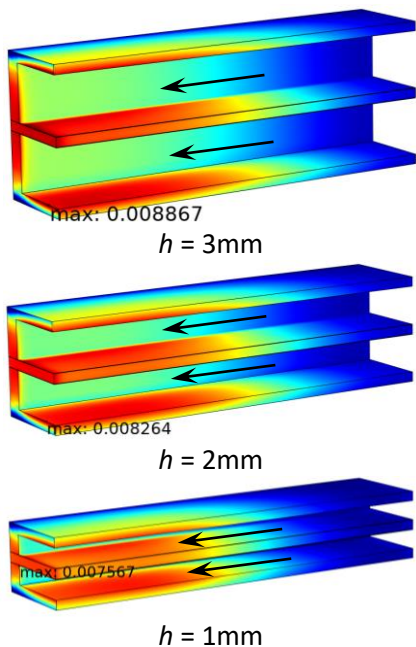

h = 3mm

h = 2mm

h = 1mm

h = 0.5mm

h = 0.25mm

(a) thermal strain

h = 3mm

h = 2mm

h = 1mm

h = 0.5mm

h = 0.25mm

(b) Von Mises stress

Fig.6 The thermal strain and Von Mises stress contour comparison of methane steam reformer under different channel heights

4. CONCLUSIONS

A three-dimensional computational fluid dynamics model coupling chemical reaction and thermal strain stress of TS-MSR has been developed. The thermo-chemo-mechanical behavior of TS-MSR processed by microchannel technology is investigated. And the following conclusions are achieved:

(1) The higher the channel height, the longer the segments with negative logarithmic mass Fourier number in the reformer. This value becomes negative when x/L exceeds 0.2 for reformer with channel height of 3mm while 0.92 for reformer with channel height of 0.25mm. It indicates decreasing the channel height of the reformer facilitates the reforming reaction from mass transfer point of view.

(2) The lower the channel height, the lower the maximum and average temperature of the reformer. The maximum temperature reaches 981K for reformer with channel height of 3mm while 939K for reformer with channel height of 0.25mm. The maximum temperature was reduced by 42K when channel height decreases from 3mm to 0.25mm. It indicates lower the maximum temperature could be achieved by decreasing channel height.

(3) High thermal strain appears in reformer catalyst layer and interconnect rib of reformer outlet section. And the higher the channel height, the higher the thermal strain. This may result in the delamination and exfoliation of catalyst layer, which could in turn cause further thermal runaway and greater strain. The corresponding maximum Von Mises stress reaches 1841MPa when channel height is 3mm while this value is 1277MPa when channel height is 0.25mm. It indicates reducing the channel height facilitate the safe operation of the reformer.

(4) Methane conversion and hydrogen yield increase first and then slightly decrease with the decrease of reformer channel height under the simulation condition. Methane conversion obtained a value of 66.4% when channel height is 3mm while this value is 83.1% for reformer with channel height of 0.5mm. The corresponding hydrogen yield value is 23.6% for reactor with channel height of 3mm while 27.7% for channel height of 0.5mm. While methane conversion is 80.1% and hydrogen yield is 26.4% for reformer with channel height of 0.25mm. With comprehensive consideration of reformer performance and safe operation, the channel height of 0.5mm was recommended.

ACKNOWLEDGEMENT

REFERENCE

[1] S. Sippel, N. Meinshausen, E.M. Fischer, E. Székely, R. Knutti, Climate change now detectable from any single day of weather at global scale, Nature Climate Change, 10 (2020) 35-41.

[2] W. Yue, Y. Li, Y. Zheng, T. Wu, C. Zhao, J. Zhao, G. Geng, W. Zhang, J. Chen, J. Zhu, B. Yu, Enhancing coking resistance of Ni/YSZ electrodes: In situ characterization, mechanism research, and surface engineering, Nano Energy, 62 (2019) 64-78.

[3] M.F. Serincan, U. Pasaogullari, P. Singh, Controlling reformation rate for a more uniform temperature distribution in an internal methane steam reforming solid oxide fuel cell, J Power Sources, 468 (2020) 228310.

[4] Z. Li, G. Yang, D. Cui, S. Li, Q. Shen, G. Zhang, H. Zhang, Modeling and evaluating of thermo-electro-chemo-mechanical behavior for pre-reformed methane-fueled solid oxide fuel cell, J Power Sources, 522 (2022) 230981.

[5] M.J. Stutz, N. Hotz, D. Poulikakos, Optimization of methane reforming in a microreactor—effects of catalyst loading and geometry, Chem Eng Sci, 61 (2006) 4027-4040.

[6] X. Zhai, S. Ding, Y. Cheng, Y. Jin, Y. Cheng, CFD simulation with detailed chemistry of steam reforming of methane for hydrogen production in an integrated micro-reactor, Int J Hydrogen Energy, 35 (2010) 5383-5392.

[7] J. Chen, L. Yan, W. Song, D. Xu, Methane steam reforming thermally coupled with catalytic combustion in catalytic microreactors for hydrogen production, Int J Hydrogen Energy, 42 (2017) 664-680.

[8] J. Chen, J. Han, D. Xu, Efficient operation of autothermal microchannel reactors for the production of hydrogen by steam methane reforming, Int J Hydrogen Energy, 44 (2019) 11546-11563.

[9] G.D. Stefanidis, D.G. Vlachos, Intensification of steam reforming of natural gas: Choosing combustible fuel and reforming catalyst, Chem Eng Sci, 65 (2010) 398-404.

[10] C. Cao, N. Zhang, D. Dang, Y. Cheng, Numerical evaluation of a microchannel methane reformer used for miniaturized GTL: Operating characteristics and greenhouse gases emission, Fuel Process Technol, 167 (2017) 78-91.

[11] Z. Li, G. Yang, S. Li, Q. Shen, F. Yang, H. Wang, X. Pan, Modeling and analysis of microchannel autothermal methane steam reformer focusing on thermal characteristic and thermo-mechanically induced stress behavior, Int J Hydrogen Energy, 46 (2021) 19822-19834.

[12] M. Zanfir, A. Gavriilidis, Catalytic combustion assisted methane steam reforming in a catalytic plate reactor, Chem Eng Sci, 58 (2003) 3947-3960.

[13] J. Shu, B.P.A. Grandjean, S. Kaliaguine, Methane steam reforming in asymmetric Pd- and Pd-Ag/porous SS membrane reactors, Applied Catalysis A: General, 119 (1994) 305-325.